Brain Stimulation 16 (2023) 1412–1424

Contents lists available at ScienceDirect

Brain Stimulation

journal homepage: http://www.journals.elsevier.com/brain-stimulation

Sub-harmonic entrainment of cortical gamma oscillations to deep brain stimulation in Parkinson's disease: Model based predictions and validation in three human subjects

James J. Sermon [a,b], Maria Olaru [c], Juan Ansó [c], Stephanie Cernera [c], Simon Little [d], Maria Shcherbakova [c], Rafal Bogacz [b], Philip A. Starr [c,1], Timothy Denison [a,b,1], Benoit Duchet [b,*,1]

[a] Institute of Biomedical Engineering, Department of Engineering Science, University of Oxford, Oxford, UK
[b] MRC Brain Networks Dynamics Unit, Nuffield Department of Clinical Neurosciences, University of Oxford, Oxford, UK
[c] Department of Neurological Surgery, Weill Institute for Neurosciences, University of California San Francisco, San Francisco, CA, USA
[d] Department of Neurology, University of California San Francisco, San Francisco, CA, USA

ARTICLE INFO

Keywords:
Sub-harmonic entrainment
Deep brain stimulation
Cortical gamma oscillations
Parkinson's disease
Wilson-Cowan model

ABSTRACT

Objectives: The exact mechanisms of deep brain stimulation (DBS) are still an active area of investigation, in spite of its clinical successes. This is due in part to the lack of understanding of the effects of stimulation on neuronal rhythms. Entrainment of brain oscillations has been hypothesised as a potential mechanism of neuromodulation. A better understanding of entrainment might further inform existing methods of continuous DBS, and help refine algorithms for adaptive methods. The purpose of this study is to develop and test a theoretical framework to predict entrainment of cortical rhythms to DBS across a wide range of stimulation parameters.

Materials and Methods: We fit a model of interacting neural populations to selected features characterising PD patients' off-stimulation finely-tuned gamma rhythm recorded through electrocorticography. Using the fitted models, we predict basal ganglia DBS parameters that would result in 1:2 entrainment, a special case of sub-harmonic entrainment observed in patients and predicted by theory.

Results: We show that the neural circuit models fitted to patient data exhibit 1:2 entrainment when stimulation is provided across a range of stimulation parameters. Furthermore, we verify key features of the region of 1:2 entrainment in the stimulation frequency/amplitude space with follow-up recordings from the same patients, such as the loss of 1:2 entrainment above certain stimulation amplitudes.

Conclusion: Our results reveal that continuous, constant frequency DBS in patients may lead to nonlinear patterns of neuronal entrainment across stimulation parameters, and that these responses can be predicted by modelling. Should entrainment prove to be an important mechanism of therapeutic stimulation, our modelling framework may reduce the parameter space that clinicians must consider when programming devices for optimal benefit.

Introduction

Deep Brain Stimulation (DBS) is a form of invasive neuromodulation, where electrical impulses are delivered to specific brain regions by implanted electrodes. In the context of Parkinson's disease (PD), high-frequency DBS (130-180 Hz) is primarily used to alleviate motor symptoms (bradykinesia, rigidity and tremor [1,2]) when medications provide inadequate benefit. While a diverse range of effects of DBS have been observed in both behaviour and neuronal rhythms, the mechanisms underlying these responses are not fully understood.

Activity in the gamma band (approximately 30 to 100 Hz) has become a target for neuromodulation as it is associated with various cognitive performance features [3] as well as motor control [4]. However, it is necessary to distinguish between broadband gamma and finely-tuned gamma (FTG). While broadband gamma reflects neuronal spiking activity over a broad frequency range (which can be as wide as 30-200 Hz), FTG represents narrowband oscillatory activity with a peak frequency between 60-90 Hz [5,6]. Here, we will be focusing on FTG oscillations, which were first revealed through invasive recordings of

* Corresponding author at: MRC Brain Network Dynamics Unit, University of Oxford, Mansfield Road, Oxford OX1 3TH, UK.
E-mail address: benoit.duchet@ndcn.ox.ac.uk (B. Duchet).
[1] These authors share senior authorship.

https://doi.org/10.1016/j.brs.2023.08.026
Received 4 May 2023; Received in revised form 28 August 2023; Accepted 30 August 2023
Available online 6 September 2023

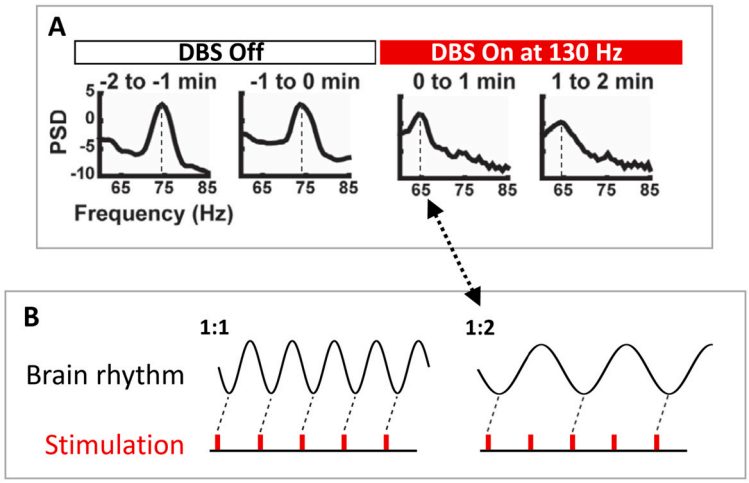

Fig. 1. Prior human recordings demonstrate 1:2 entrainment of cortical gamma rhythms from subcortical stimulation. (A) PSD of gamma band activity recorded from the motor cortex before and during DBS to the STN at 130 Hz. In the DBS Off state, a natural ~75 Hz gamma rhythm can be observed. This is entrained at 65 Hz during the following two minutes of DBS On at 130 Hz. (B) 1:1 entrainment corresponds to one stimulation pulse per brain rhythm cycle and a rotation number of 1, 1:2 entrainment corresponds to two stimulation pulses per brain rhythm cycle and a rotation number of 0.5. Hence, during 1:2 entrainment, the brain rhythm locks to a frequency of half that of the external stimulation. This corresponds to the DBS On state of panel A. Panel A is adapted from [5] (with no permission required).

the basal ganglia in PD patients on antiparkinsonian medications [7,8]. These have been thought to represent a "prokinetic" brain rhythm, in contrast to "antikinetic" beta rhythms (13-30 Hz). Recently, prominent FTG oscillations have been found during invasive recordings from motor cortical areas in PD [5,9,10], and may be associated with dyskinesias. Additionally, similar cortical oscillations have been observed in rat models of dyskinesia [11,12].

Entraining FTG in patients with PD has potential to be beneficial (in the absence of dyskinesia). Transcranial alternating current stimulation (tACS) at gamma frequency was observed to increase motor velocity in PD, while tACS at beta frequency saw it decrease [13]. It was hypothesised that entrainment (specifically 1:1 entrainment at stimulation frequency, as depicted in Fig. 1B) of both gamma and beta oscillations would explain this observation by enhancing "prokinetic" and "antikinetic" rhythms, respectively. Additionally, a shifted FTG peak frequency has been noted in the motor cortex in response to high-frequency DBS of the STN [5,14,10]. The gamma peak, off-stimulation between 65 and 80 Hz, locks to the half harmonic of stimulation (see Fig. 1), corresponding to 1:2 entrainment. Together, these studies suggest that the entrainment of FTG by DBS could play a role in ameliorating PD-associated motor symptoms. Moreover, the half-harmonic lock indicates that the response to stimulation is complex and goes beyond entraining rhythms solely at the frequency of stimulation or suppressing them. However, there is currently no theoretical understanding of 1:2 gamma entrainment in PD and generally no framework to predict the occurrence of specific entrainment regimes in response to brain stimulation.

In this study, we use a model-based approach that utilises chronic invasive cortical recordings in PD patients to predict the properties of entrainment of cortical activity by basal ganglia DBS. We postulate that by constraining the parameters of a neuronal population model, it will be possible to predict stimulation parameters that lead to 1:2 gamma entrainment for patients with off-stimulation (medication induced) FTG. We provide a theoretical introduction to 1:2 gamma entrainment through the concepts of Arnold tongues (regions of entrainment in the stimulation frequency and amplitude space) and rotation number (the ratio of the average number of oscillation cycles to stimulation pulses). We proceed to develop a patient-specific approach by fitting a model representing interacting neural populations, the Wilson-Cowan model, to features of invasive chronic electrocorticography (ECoG) data recorded off stimulation from patients with PD. Using the fitted-models, we predict the regions of 1:2 entrainment in the stimulation parameter (frequency and amplitude) space. We proceed to verify key features of the 1:2 entrainment regions with follow-up recordings from the same patients. Lastly, these results are discussed and the implications are highlighted for future stimulation therapies.

Materials and methods

Arnold tongues and rotation number

The frequency locking (entrainment) behaviour of a neural rhythm to external stimulation across stimulation frequency and amplitude can be described by Arnold tongues [15]. Arnold tongues are the regions in the stimulation frequency and amplitude space where frequency-locking occurs. Frequency locking is observed when a rotation number of the form p:q, where p and q are coprime integers (i.e. no integer other than 1 divides both p and q), is maintained for several stimulation periods. In general, the rotation number may not be a ratio of integers (it is a ratio of integers only when there is frequency locking), and corresponds to the average number of oscillatory cycles achieved by the rhythm between two periodic pulses of the driving stimulation. This is calculated for periodic signals as

$$\frac{\theta_N - \theta_0}{2\pi N}, \tag{1}$$

where θ_N is the phase after N stimulation pulses (in this study, $N > 50$) and θ_0 is the initial phase. Previously, Arnold tongues have been used to describe 1:1 entrainment in response to noninvasive neuromodulation [16–19]. Depending on the system considered and the stimulation waveform, Arnold tongues can theoretically exist for various rotation numbers, including p:q with large p and/or q. However, in real systems, often only the tongues corresponding to the most stable rotation numbers, with low p and q values, will be observed. Arnold tongues often have different shapes for different dynamical systems. Generally, an Arnold tongue expands in width across larger frequency ranges as stimulation amplitude increases. This continues up until an amplitude where the tongue may border a region with another frequency-locking ratio or lose entrainment altogether.

The model we use to predict 1:2 entrainment based on off-stimulation recordings only is introduced next. How Arnold tongues are obtained in this model is described later in the *Providing stimulation and entrainment analysis in the model* section.

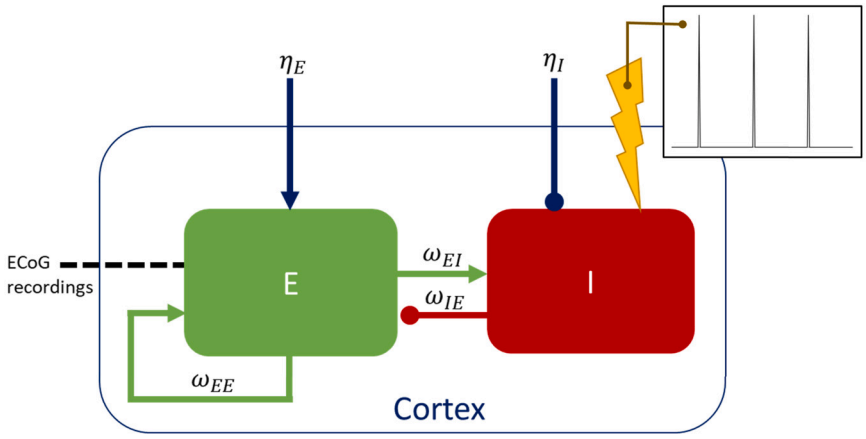

Fig. 2. The two-population Wilson-Cowan model. Stimulation is applied to the inhibitory population (I) and data recorded from the excitatory population (E). The weights of the three connections present in this model are ω_{EI} (excitatory connection from E to I), ω_{IE} (inhibitory connection from I to E), and ω_{EE} (self-excitatory connection from E to E). Additionally, there are external inputs, η_E and η_I, to each population. The insert displays the single time step stimulation pulse with no recharge used throughout this study (pulses with different active recharge durations, and with passive recharge are considered in Supplementary Materials section E.2).

Wilson-Cowan model

The Wilson-Cowan model is well-suited to fit population-level brain recordings. The Wilson-Cowan model is a mean-field model describing interacting neuronal populations [20,21] and, hence, is a natural choice to represent off-stimulation ECoG recordings and predict 1:2 gamma entrainment. While the sine circle map, a simpler model, can provide a first level description of 1:2 gamma entrainment (see Supplementary Materials section D), it only represents a single neural oscillator and cannot fit population-level brain recordings. The Wilson-Cowan model has been used in the analysis of neuronal responses to periodic and varying stimulation [22–26] and in theoretical studies of entrainment [27,28]. Additionally, the model has been used in the analysis of resonances [29], as well as in the communication of information [30]. The Wilson-Cowan model has a limited number of parameters which makes it feasible to constrain the model with a low risk of over-fitting the data. Despite the relatively small number of parameters, it is also able to capture a wide variety of dynamics [31,32,27].

We use the two-population Wilson-Cowan model to represent excitatory and inhibitory cortical populations with reciprocal connections (see Fig. 2). We do not include subcortical populations in this model, and assume that subcortical stimulation is transmitted unperturbed to the cortex. The Wilson-Cowan model can be used to predict the interactions of large groups of neurons and outputs the activity of an excitatory and an inhibitory population. The population activities are denoted by E and I, respectively, and are proportional to the firing rate of that population's neurons. Stochastic differential equations describe the evolution of E and I as

$$dE = \frac{1}{\tau_E}\left[-E + f\left(\eta_E + \omega_{EE}E + \omega_{IE}I\right)\right]dt + \zeta dW_E,$$

$$dI = \frac{1}{\tau_I}\left[-I + f\left(\eta_I + \omega_{EI}E\right) + A_{stim}(t)\right]dt + \zeta dW_I,$$

$$f(x) = \frac{1}{1+e^{-b(x-1)}}.$$

These interactions are weighted by coupling strengths denoted ω_{PQ} (going from population P to population Q), and occur through a sigmoid function f of steepness coefficient b. τ_E and τ_I represent the time constants of the excitatory and inhibitory populations, respectively. η_E and η_I are the constant inputs to the respective populations. Stochasticity is introduced to the model through Wiener processes, W_E and W_I, with noise standard deviation denoted by ζ. Noise is required to reproduce the off-stimulation data, which is characterised by bursts of activity rather than perfectly periodic dynamics (see Fig. 5D).

It is unclear whether the effect of subcortical stimulation on the motor cortex is excitatory or inhibitory (more details in the Discussion section). In this study of the cortical response, we model the effect as inhibitory by applying periodic high-frequency stimulation, $A_{stim}(t)$, to the inhibitory population, while the ECoG local field potential (LFP) is modelled as the activity of the excitatory population. However, we also verify in Supplementary Materials section E.5 that our results hold for stimulation applied to the excitatory population and ECoG LFP obtained as the activity of the inhibitory population. Additionally, stimulation is applied directly to the inhibitory population, not through the sigmoid function, as this provides a greater wealth of dynamics by avoiding saturation effects [26].

Data collection

Human neural data were collected from three patients with Parkinson's disease (Table 1). Cortical data off-stimulation were collected to fit the Wilson-Cowan model. On-stimulation data (subcortical stimulation) at variable stimulation frequencies and amplitudes were then used to validate predictions from the fitted model. Patient clinical symptoms assessed 90 days pre-operation are summarised in Supplementary Materials Table B.

Patients were selected for participation in this study based on the presence of a peak in gamma band activity in the primary motor cortex off-stimulation (which is a necessary condition to fit a model to off-stimulation gamma activity). Patients were diagnosed with idiopathic Parkinson's disease by a movement disorders neurologist and underwent DBS surgery of either the subthalamic nucleus (STN) or globus pallidus (GP). Target choice was based on the patients' neuropsychological test results, which indicated pallidal implantation for patients with mild cognitive impairment or history of clinical depression [33,34]. Patients were bilaterally implanted with the Medtronic Summit RC+S bidirectional neural interface (clinicaltrials.gov identifier NCT03582891, USA FDA investigational device exemption number 180097, IRB number 18-24454) quadripolar cylindrical leads into subcortical nuclei (Medtronic model 3389 or 3387 for STN and pallidum, respectively), and subdural paddle-type leads over the primary motor cortex in the subdural space (Medtronic model 0913025), see Fig. 3A1-3 for RCS02, Fig. 3B1-3 for RCS10 and Fig. 3C1-2 for RCS18. Implantations of subcortical leads were performed using frame-based stereotaxy, and confirmed by intraoperative cone beam CT and microelectrode recording (MER) in the awake state using standard methods in RCS02 and RCS10 [35], and by intraoperative cone-beam CT alone in RCS18 [36]. For RCS10, the active contact array was localised in the GP using MER mapping

Table 1
Patient information summary. LEDD: levodopa equivalent daily dose, UPDRS: Movement Disorders Society Unified Parkinson's Disease Rating Scale, UPDRS (off-on): percent change off vs on medication, STN: subthalamic nucleus. "Time of charting" refers to on-stimulation data collection to test model predictions. *RCS18's right lead was deactivated during testing since it was recently reimplanted and undergoing clinical optimisation.

Patient	RCS02	RCS10	RCS18
Age (years)	54	64	67
Disease Duration (years)	7	13	7
Gender	M	F	M
LEDD (mg/day)	1425	1083	2031
UPDRS-III off med	49	89	49
UPDRS (off-on)	90%	53%	76%
DBS Target	STN	Pallidum	STN
Duration of chronic DBS prior to collection of entrainment data (months)	30	10	7
Clinical Stimulation Settings	R: 1-C+, 2.6 mA, 60 μs, 130 Hz L: 2-C+, 2.4 mA, 60 μs, 130 Hz	R: 1-2-C+, 5.0 mA, 90 μs, 150 Hz L: 2-C+, 5.0 mA, 90 μs, 150 Hz	R: 2-C+, 2.3 mA, 60 μs, 130 Hz L: 2-C+, 2.4 mA, 60 μs, 130 Hz
Titration Ranges	R/L: Freq.: 110-170 Hz, Amp.: 0.7-3.1 mA	R/L: Freq.: 130-150 Hz, Amp.: 0-6.5 mA	R: OFF* L: Freq.: 40-180 Hz, Amp.: 0.9-4.3 mA

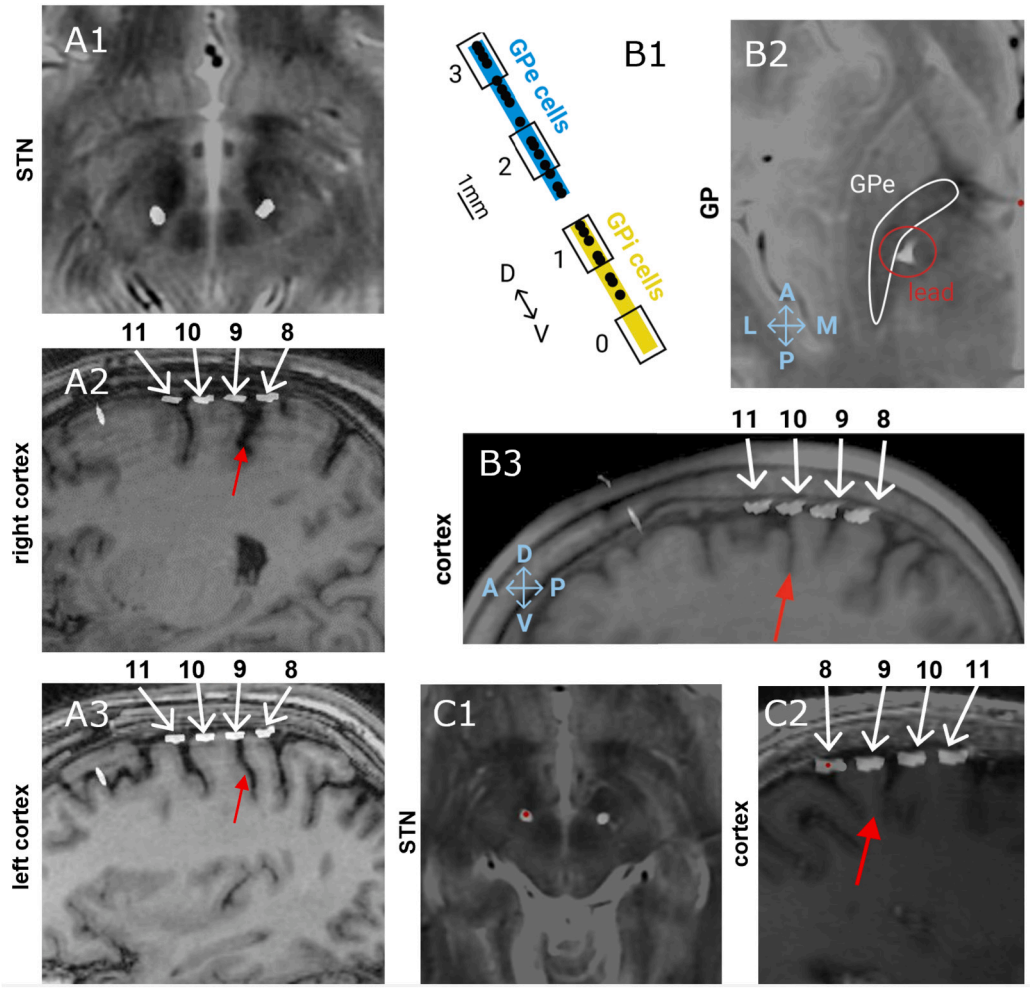

Fig. 3. Contact localisation across the three subjects. The patients are presented as RCS02 (A1-3), RCS10 (B1-3) and RCS18 (C1 and 2). (A1-3, B2-3, C1-2) Localisation of contacts with a postoperative CT scan that is computationally fused with the preoperative planning MRI scan. (A1 and C1) subthalamic nucleus (STN) lead on a T2-weighted MRI scan. In C1, the red dot indicates the left STN lead. (A2-3, B3, C2) Quadripolar subdural paddle lead on sagittal T1-weighted MRI shows the relationship between the central sulcus (red arrow) and contacts (white numbered arrows). For RCS10 (A2-3) and RCS18 (C2), contacts 11 and 10 were both over the pre-central gyrus whereas contact 9 was on the post-central gyrus. RCS02 (B3) was implanted slightly more anteriorly and contacts 9 and 10 were on the pre-central gyrus and 11 on the superior frontal gyrus. (B1) globus pallidus (GP) contact localisation (black numbered rectangles) with respect to the boundaries of the internal globus pallidus (GPi) (yellow) and external globus pallidus (GPe) (blue) as defined by micro-electrode recording mapping of single-unit cells (black dots). (B2) GP lead on an axial T2-weighted MRI, which visualises the GP as regions of T2 hypointensity (GPe highlighted by a white contour).

of single-unit cells to traverse the postero-lateral regions of the external globus pallidus (GPe) and globus pallidus internus (GPi), Fig. 3B1. For RCS02, the motor territory of the STN was confirmed by eliciting movement-related single-cell discharge patterns during MER when the DBS lead was placed with the middle two contacts in dorsal STN. Surgical placement of subdural cortical paddles has been previously described in detail [37]. Similar to subcortical contacts, localisation of subdural paddles was confirmed by computationally fusing a postoperative CT scan to the preoperative planning MRI scan, Fig. 3B1-3, A2-3 and C1-2.

Prior to the initiation of standard therapeutic DBS, we recorded four-channel LFPs of the cortical, and pallidal (n = 1) or subthalamic (n = 2) sites of each hemisphere between two and four weeks post implantation. The data were streamed from patients during normal activities of daily living and while on their schedule of antiparkinsonian medication. Only the cortical prestimulation data were used to fit the Wilson-Cowan model. The recording methods and data processing were similar to those described by Gilron et al. [10]. Briefly, neural data were recorded from subcortical (STN or GP, as per patient's DBS target; Fig. 3A1, B2, C1) and cortical (contact pairs 11-9 and 10-8 for RCS02, Fig. 3A2-3; 11-10 and 9-8 for RCS10 and RCS18, Fig. 3B3, C2) sensing electrodes via a patient-facing graphical user interface application. Neural data were collected at 250 Hz. The Summit RC+S has two onboard filters applied after digitisation that were set to a high pass of 0.85 Hz and a low pass of 450 Hz before amplification followed by 1700 Hz low pass filter after amplification.

After several months of continuous subthalamic (n = 2) or pallidal (n = 1) stimulation at clinically optimised parameters, we conducted a follow-up in-clinic recording session with each subject in their on-medication state to validate the initial model predictions. During recordings, we cycled through a range of stimulation frequencies and amplitudes to further explore the DBS parameter space (Table 1). In each participant, we delivered stimulation at their clinical contact in the STN or GP, while recording from cortical sensing contacts 11-10 and 9-8. In each trial, we tested a single frequency-amplitude combination for 30 seconds while the patient was at rest. Sessions lasted two to three hours, and the number of data points collected was different in each patient due to patient fatigue. While it is not clear if fatigue plays into 1:2 entrainment, the testing order of stimulation parameters was not predetermined, making the point at which each tongue boundary was tested effectively random. In particular, the top tongue boundaries were not tested only later in the sessions when we would expect fatigue to be higher. It should also be acknowledged that non-stationary medication levels, associated with intermittent medication intake, could affect 1:2 entrainment at certain stimulation parameters. Filter settings for cortical contacts were the same as during off-stimulation recordings.

Fitting process

To fit the parameters of our Wilson-Cowan model to prestimulation cortical FTG, we processed the off-stimulation cortical recordings (over three hours for each subject, collected between two and four weeks post implantation) to obtain data features for each patient. We separated the off-stimulation sessions into epochs with a minimum of 30 seconds of continuous and uninterrupted recordings. Longer uninterrupted recordings were not consistently available in some of the patients due to packet losses during streaming. However, 30-second epochs were sufficient to capture stable FTG properties. For the fitting process, we only used one epoch for each patient which was selected by identifying the epoch with the most prominent cortical gamma peak (to maximise signal-to-noise ratio) within the frequency range ±3 Hz of the approximate average peak gamma frequency of the overall dataset, i.e. 75 Hz for RCS02 and RCS10, 78 Hz for RCS18 (the ±3 Hz frequency range captured all variation in off stimulation FTG frequencies in each dataset). From this epoch, the signal was band-passed between ±3 Hz of the gamma peak (the band-pass width was chosen to capture the whole width of the FTG peak). Three features were selected for the purposes of fitting the model to each patient; the power spectral density (PSD) of the cortical FTG signal, its envelope PSD, and its envelope probability density function (PDF). These features are shown for RCS10 in Fig. 4A1-3, and for RCS02 and RCS18 in Fig S.2 in Supplementary Materials. The envelope is the modulus of the analytical signal of the band-passed recording and refers to a curve that traces the upper bound of the signal, providing a measure of the oscillation's amplitude. The envelope PDF represents the distribution of the values of the envelope over the duration of the signal. These features were selected to provide a representation of the signal and its envelope in the frequency domain, as well as a representation of the statistics of the envelope in the time domain. We demonstrate in Supplementary Materials section A.1 that there is little correlation between the three features mentioned here, and that all three features are required to capture the full dynamics of the data. Fitting to off-stimulation features ensured that any presence of 1:2 entrainment is not predetermined, as could have been the case if fitting to on-stimulation data. The bipolar contact pairs used for fitting were 11-9 in RCS02, and 11-10 in RCS10 and RCS18. In all cases, at least one of the contacts was localised over the pre-central gyrus (see Fig. 3A2, A3, B3, and C2). Contact pairs were selected for the fitting process of each patient by which pairs had the most consistent gamma power over time.

Model parameters were then optimised to best match the selected cortical FTG data features (Fig. 4A1-3). This process follows a fitting methodology similar to [26,38], repeated for each patient. It begins by generating random sets of parameters, and selecting parameter sets with a PSD broadly similar to that of the data (the first loop of Fig. 4B), i.e. with a gamma peak between 70 to 80 Hz. This improves the computational efficiency of the parameter fitting. Accepted parameters enter an optimisation loop (the second loop of Fig. 4B) using the patternsearch function of Matlab2020b, which minimises the cost function capturing the distance between model and data features (see Supplementary Materials section A.2). We run this optimisation to obtain approximately 2500 parameter sets fitted to the 30 seconds of off-stimulation cortical data, each corresponding to a different local minimum of the cost function. From the resulting fits, we select the 20 with the greatest R^2 values and perform further simulations to refine the ranking of the fits (the third loop of Fig. 4B), more details can be found in Supplementary Materials section A.3. The top-ranked fit is then selected based on these simulations. We don't expect overfitting to be an issue given that we are fitting to off stimulation data, where there is no entrainment in the signal. Predictions of the response to external stimuli are then made by introducing stimulation to the off-stimulation fitted model.

Providing stimulation and entrainment analysis in the model

We obtain entrainment predictions in the model (i.e. Arnold tongues, in particular the 1:2 Arnold tongue) by providing high-frequency DBS at variable stimulation amplitudes and frequencies. The stimulation pulse provided throughout the majority of the modelling work in this study, unless mentioned otherwise, is a single time step positive pulse with no recharge (see the insert in Fig. 2). This stimulation pulse was chosen for simplicity. Different recharge lengths and stimulation waveforms are explored in Supplementary Materials sections E.2 and E.3. Stimulation is introduced in the model as described in the *Wilson-Cowan model* section.

In the presence of stimulation, entrainment is assessed in the model by computing the rotation number using equation (1) where θ_i is taken as the unwrapped Hilbert phase of the excitatory population activity after i stimulation pulses. This was calculated over 50 stimulation cycles and averaged over five repeats at each stimulation parameter. To compare with data, the PSD of the model output with stimulation applied was calculated using Welch's PSD estimate over the same number of stimulation cycles and repeats as the rotation number. The peak PSD

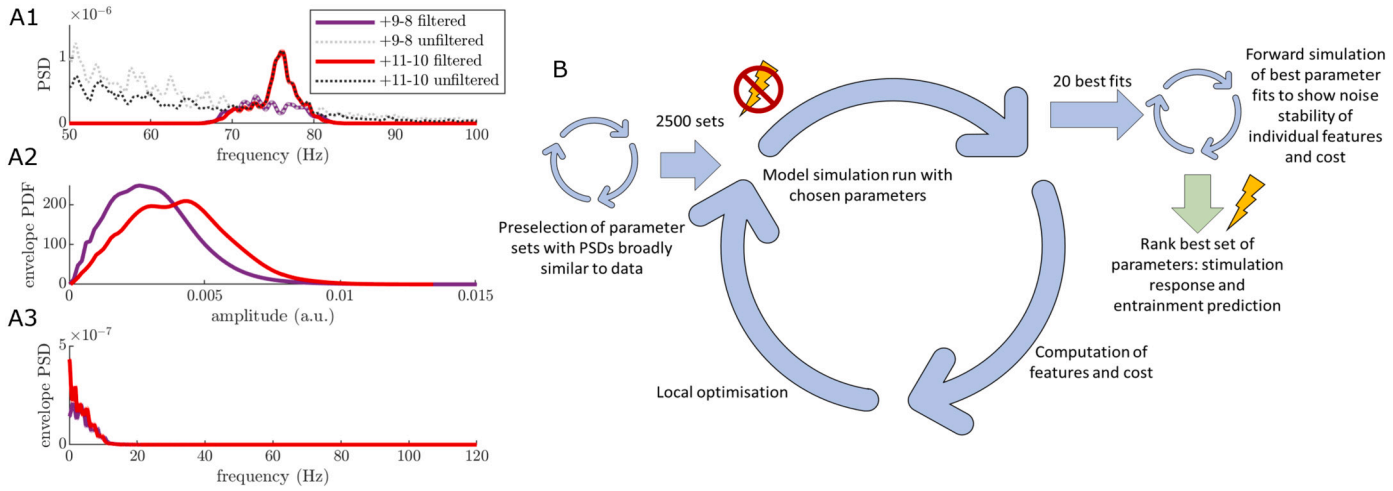

Fig. 4. Use of prestimulation human cortical recordings to fit Wilson-Cowan model parameters. (A1-3) The three data features from RCS10 off-stimulation cortical recordings: power spectral density (PSD) (A1), envelope probability density function (PDF) (A2) and envelope PSD (A3), for the selected epoch, based on the gamma peak height in the cortical 9-8 and 11-10 contact pairs. The features shown are from the cortical contacts as labelled in Fig. 3B3. The solid red and purple lines display the band-pass filtered cortical signals between 72 Hz and 78 Hz, as the peak occurred at 75 Hz for this patient. The black and grey dotted lines in the PSD plot show the unfiltered cortical signals. The unfiltered signal for the 11-10 contact pair still displays the FTG peak seen in the filtered data. The fitting is based off the filtered data from the 11-10 contact pair. (B) The optimisation pathway for fitting the model to off-stimulation data. This process is broken down into three main loops, as discussed in the *Fitting process* section. Once a fitted set of model parameters is obtained we are able to make predictions for the neuronal population responses in the on-stimulation state.

was calculated as the maximum power in the 0 to 200 Hz frequency range.

Entrainment analysis of the ECoG recordings

Entrainment of cortical FTG to DBS was assessed in the data using a spectral method since the rotation number cannot be reliably computed in the data. The PSD of the data (from the bipolar recordings based on cortical contacts 11-9 in RCS02 and cortical contacts 11-10 in RCS10 and RCS18) was calculated in a similar way to that of the model, using Welch's PSD estimate. Only frequencies recorded within the 40 to 120 Hz range were considered when computing the peak power. To determine whether each set of stimulation parameters achieved entrainment we first determined the approximate PSD slope on stimulation by averaging the PSD in the ranges $[f_s/2-10, f_s/2-5]$ and $[f_s/2+5, f_s/2+10]$, where f_s denotes stimulation frequency. These ranges were chosen to avoid spectral changes around the half harmonic. The signal was then determined to be showing 1:2 entrainment if the height of the PSD at half the stimulation frequency was over three times greater than the approximated baseline expected from the measured slope. This placed the threshold over any variation due to noise. The threshold was chosen such that there was very little variation in the results when increasing it, and provided a conservative assessment of entrainment (less likely to lead to spurious entrainment than a lower threshold such as three standard deviations of the noise).

Correspondence between stimulation amplitude in the model and in the data

While the stimulation frequency unit is the same in the model and the data (Hz), the stimulation amplitude unit is arbitrary in the model. To correlate peak PSD predictions in the model and the data, it is therefore a pre-requisite to establish a correspondence between stimulation amplitude in the model and in the data. This was done by selecting the scaling of the model stimulation amplitude axis that maximised the correlation of peak PSD of 1:2 entrained points (as assessed in the data) between the data and the model (grid search over a linear scale).

Optimising the scaling of the model stimulation amplitude introduces an additional free parameter which needs to be accounted for in statistical analyses. For each patient, significance of the correlation between peak PSD predictions in the model and the data is therefore assessed using an approximation of the distribution of correlation coefficients under the null hypothesis (no correlation) obtained from 10,000 permutations. For each patient, we randomly reassign PSDs from the data to the different stimulation parameters used. Each permutation is then compared against model PSD predictions and the scaling is optimised to maximise the correlation between the peak PSD at the half harmonic of stimulation frequency between the model and the data, as outlined above. Only permutations which resulted in at least five 1:2 entrained results from the model simulations were accepted. This was to avoid spurious correlations in the surrogate distribution that would result from a very low number of datapoints. Placing the threshold at five is also conservative as all patient datasets have more than five entrained points. P-values are then calculated using the resulting (approximately) normal distribution of correlation coefficients.

Results

We fitted the Wilson-Cowan model, a model of interacting neuronal populations, to prestimulation ECoG recordings in three patients with PD. Using the fitted models, we predicted for each patient the stimulation parameters leading to 1:2 entrainment of FTG. We then verified these predictions in follow-up on-stimulation recordings from the same patients.

Prediction of 1:2 entrainment of FTG using a fitted Wilson-Cowan model

For all patients, the Wilson-Cowan model fitted to the patient's prestimulation cortical FTG successfully reproduced all three FTG features. The top ranked model parameter sets (Table A in Supplementary Materials) had average R^2 values (across 50 simulations) of 0.961, 0.944 and 0.868 for RCS02, RCS10 and RCS18 respectively, with good or satisfactory fits across all three features (Fig. 5 for RCS10, and Fig S.3 in Supplementary Materials for RCS02 and RCS18). The fitted models oscillate at the patient's FTG natural frequency (between 75-80 Hz in the absence of stimulation), as seen in Fig. 5A for RCS10, and Fig S.3A1 and B1 in Supplementary Materials for RCS02 and RCS18.

In the presence of low amplitude stimulation, all three models display a 1:2 Arnold tongue (i.e. entrainment region) around a stimulation

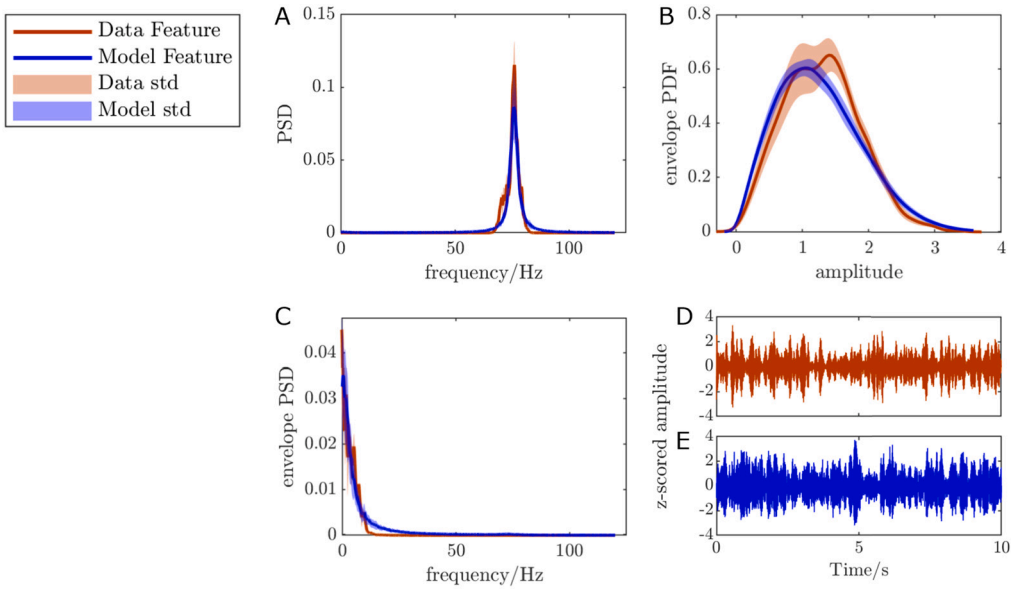

Fig. 5. Comparison of the cortical FTG features from z-scored data and the features from z-scored model output of the best ranked model parameter set for RCS10. $R^2 = 0.944$ on average across 50 simulations lasting 100 seconds each. The model closely matches the data PSD (A), envelope PDF (B), and envelope PSD (C). (D-E) Comparison of the band-passed off-stimulation time series from patient data (D) and model output (E) show that the model is capable of replicating similar time-domain dynamics. In all panels, the data is in red, and the model in blue.

frequency between 150-160 Hz (the 1:2 tongue stems from twice the natural frequency of the model). This is shown by the green 1:2 Arnold tongue in Fig. 6A, D and G, which correspond to a region of 1:2 entrainment (constant rotation number of 0.5). The 1:2 Arnold tongue is bordered by a larger zone of 1:1 entrainment, indicated by the red regions. When stimulation is provided at 130 Hz (indicated by the black line), the excitatory population can be entrained at 65 Hz for a range of stimulation amplitudes. In all three fitted models, the 1:2 tongue is left leaning (more of the tongue is to the left of the frequency it stems from, see Fig. 6A, D and G), which suggests that stimulation frequencies lower than the stem of the tongue are more likely to lead to 1:2 entrainment. The range of stimulation frequencies that can give rise to 1:2 entrainment (given an appropriate stimulation amplitude) is the narrowest in RCS02 (110-160 Hz), and the broadest in RCS18 (60-160 Hz). In all cases, we note that increasing stimulation amplitude above a certain value will result in the loss of 1:2 entrainment.

The left lean of the 1:2 Arnold tongues does not depend on whether stimulation is applied to the inhibitory population or the excitatory population (see Supplementary Materials section E.5). Additionally, the 1:2 entrainment region exhibits a left lean regardless of whether the stimulation being applied is in the form of a single time step pulse train, pulse trains with various recharge durations or more complicated waveforms (see Supplementary Materials sections E.2 and E.3).

Additionally, the fitted Wilson-Cowan models predict that the highest spectral peaks will occur at the lowest frequencies for which 1:2 entrainment arises, as seen in Fig. 6B, E and H.

Validation of model predictions in human patients during chronic therapeutic stimulation

The presence of 1:2 entrainment at variable stimulation parameters was investigated in follow-up recordings for the same patients as the Wilson-Cowan model was fitted to (see recording details in the *Data Collection* section). These data were only examined following the core predictions from the model.

Left lean of the 1:2 tongue, and loss of entrainment for large stimulation amplitudes For all three patients, the data show regions of stimulation parameters for which 1:2 entrainment can be observed (Fig. 6C, F and I), and these Arnold tongues appear to exhibit overall similar shapes to the Wilson-Cowan model predictions (shown in Fig. 6A, D and G). For RCS10, while 1:2 entrainment was seen for amplitudes greater than 5.5 mA for 140 and 130 Hz, it was lost for 150 Hz (Fig. 6F). This is a robust observation as three repeats led to the same outcome for this particular combination of stimulation parameters (150 Hz, 5.5 mA, labelled 2 in Fig. 6F). Hence, the 1:2 tongue has a left lean in this set of data with 1:2 entrainment being maintained at higher amplitudes for lower frequencies of stimulation, which is also the case in the model (Fig. 6D). RCS18 also exhibits a left-leaning 1:2 tongue. There is no 1:2 entrainment at 2 mA for stimulation frequencies above 150 Hz, however, in the range of 50-140 Hz we can see 1:2 entrainment up to 4 mA (Fig. 6I). This forms part of the top boundary of the 1:2 Arnold tongue. Additionally, there is a boundary to the right of the 1:2 tongue where no entrainment is seen for any amplitude with stimulation frequencies greater than 155 Hz. We are also able to see loss of entrainment on the lower left boundary from 50-150 Hz to further demonstrate the left lean. The corresponding model also predicts 1:2 entrainment down to 60 Hz in Fig. 6G, which is not seen in all other model predictions and is further supported by the data (Fig. 6I). Due to patient fatigue, we were unable to chart the right boundary of the 1:2 tongue in RCS02 (Fig. 6C). Hence, we are unable to determine if this patient does exhibit a left lean from their data. However, the 1:2 tongue of the model prediction for RCS02 (Fig. 6A) is smaller than the other model predictions, with a significantly lower top boundary (stimulation amplitude at which 1:2 entrainment is lost, around 3.5 mA). This can also be seen in the corresponding data (Fig. 6C).

Change in entrained gamma power with stimulation frequency and amplitude Overall, the data validate the model's prediction of highest power for the lower frequencies within the 1:2 tongue. In RCS10, changing stimulation parameters from 130 Hz, 6.5 mA to 150 Hz, 5 mA results in a drop in entrained peak power, as indicated by the colourscale in Fig. 6F. The increase in PSD with decreasing stimulation frequency ($p<1\times10^{-4}$, Fig. 7C) and increasing stimulation amplitude ($p<0.05$, Fig. 7D) are statistically significant. RCS18 also displays a statistically significant increase in entrained peak power as stimulation frequency is decreased ($p<0.001$, Fig. 7E) and stimulation amplitude is increased ($p<1\times10^{-9}$, Fig. 7F). Power changes with stimulation parameters do not show sta-

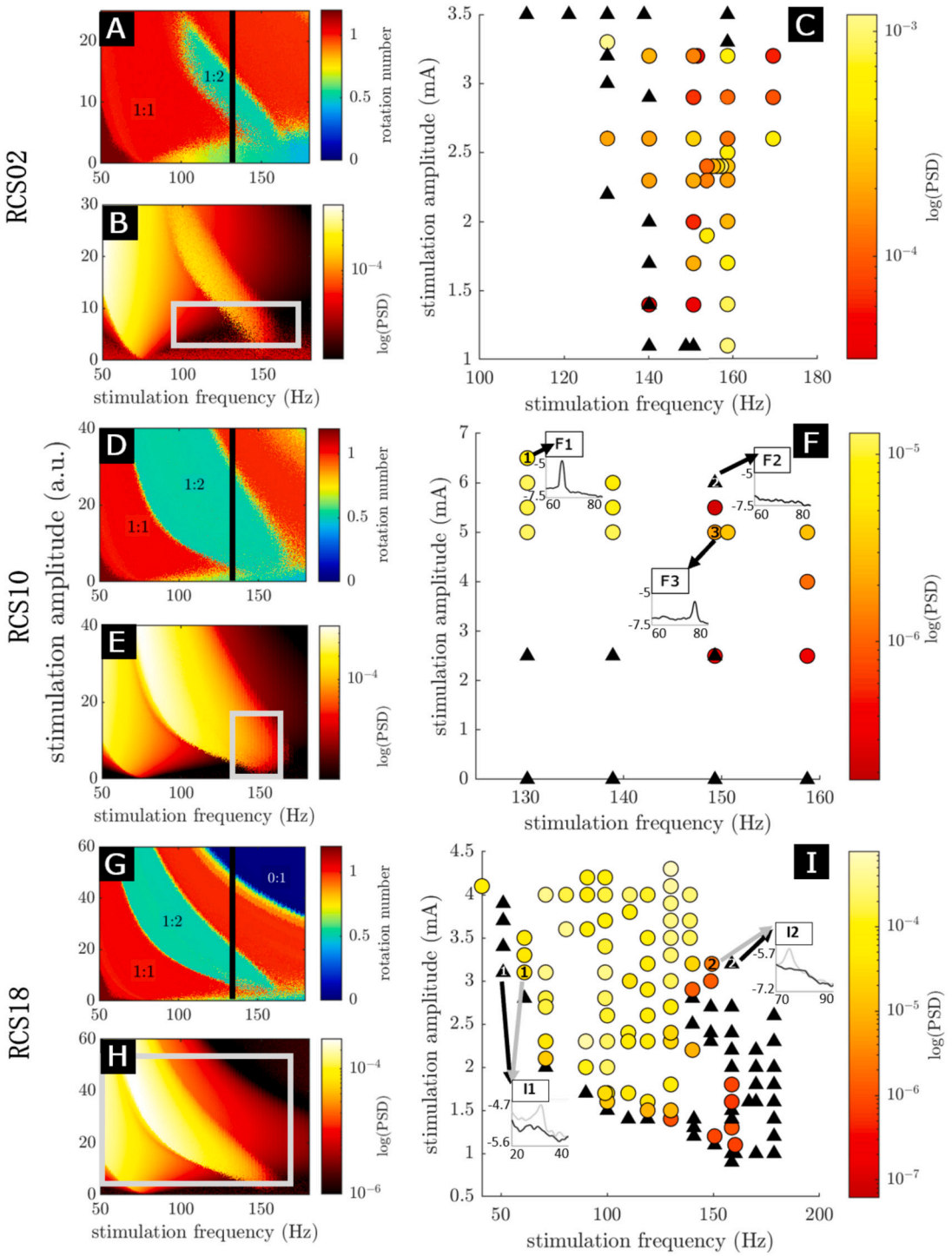

Fig. 6. Testing model predictions of a cortical circuit's response to an external stimulus using human neural data during neurostimulation. Stimulation frequency is the horizontal axis for all panels, while stimulation amplitude is the vertical axis for all panels. Stimulation amplitude has arbitrary units (a.u.) for all model panels (A, B, D, E, G, and H) and is in mA for the data panels (C, F and I). Panels A-C are for RCS02, D-F for RCS10 and G-I for RCS18. Panels A, D and G have colour scales indicating the rotation number (as explained in the *Arnold tongues and rotation number* section) resulting from the stimulation parameters at that point, where 1:1 entrainment is in red and 1:2 entrainment is in green. For these panels, the black line indicates the 130 Hz stimulation condition used in [5,14]. (A, D, G) The entrainment field of the Wilson-Cowan model with the top ranked parameters. The stimulation applied is a single time step pulse with no recharge. (B, E, H) The maximum height of the entrained peaks as predicted by the top-ranked Wilson-Cowan model fit, calculated as laid out in the *Providing stimulation and entrainment analysis in the model* section. The grey rectangles indicate comparable stimulation parameter ranges to those used in the variable stimulation response data, with stimulation amplitude scaling calculated as outlined in the *Correspondence between stimulation amplitude in the model and in the data* section. (C, F, I) The height of entrained peaks obtained from patient recordings for a series of different stimulation parameters. Circles display peak height (represented by the colour scale) of parameters that displayed entrainment (as seen e.g. in insert F1), while black triangles are for parameters that did not display entrainment (as seen e.g. in insert F2). The occurrence of both a black triangle and a circle at the point (140 Hz, 1.4 mA) in panel C and point (150 Hz, 2.5 mA) in panel F indicate intermittent entrainment, hence, this will likely be on the boundary of the tongue. Inserts F1-3 and I1-2 show the logarithm of PSDs over frequencies around half the stimulation frequency. For inserts I1-2 the grey arrow and line indicate stimulation parameters where 1:2 entrainment was observed and black where it was not.

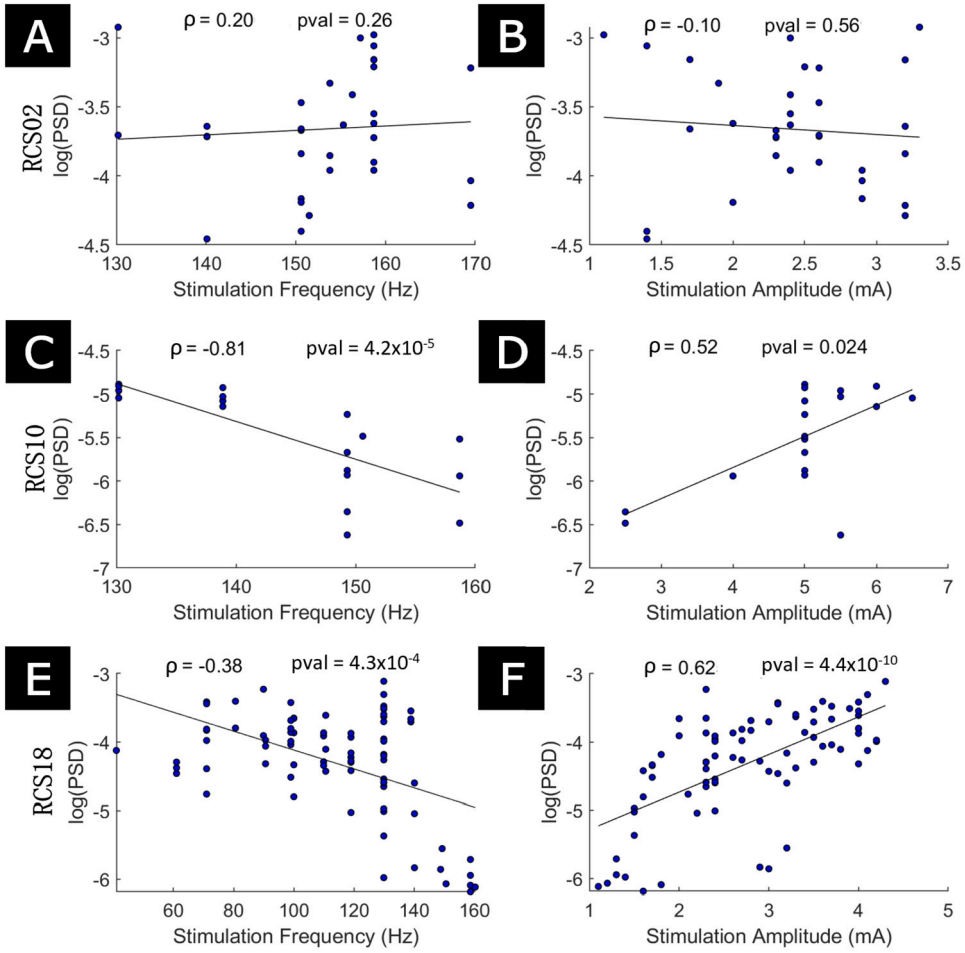

Fig. 7. 1:2 entrained power correlates with stimulation parameters in two out of three patient datasets. The results for RCS02, RCS10, and RCS18 are presented in the first row, second row, and third row, respectively. The first column displays the comparison of the 1:2 entrained PSD peak heights against stimulation frequency, with stimulation frequency acting as the sole predictor of the linear regression. The second column shows the comparison of the 1:2 entrained PSD peak heights against stimulation amplitude, where stimulation amplitude acts as the sole predictor of the linear regression. In all panels, datapoints considered are stimulation parameter combinations that resulted in 1:2 entrainment. The correlations are Spearman's.

tistically significant trends within the 1:2 tongue in RCS02 (Fig. 7A-B). The increase in entrained peak power with decreasing stimulation frequency in RCS10 and RCS18 is in agreement with model predictions. The increase in entrained peak power with increasing stimulation amplitude is also consistent in the data and the model across the 1:2 tongue, but the relationship reverses in the model when controlling for stimulation frequency (see Fig. 6B, E, and H). This is likely to also be the case in the data, although there aren't enough data points to run a statistical analysis for RCS10.

Comparing model predictions of entrained peak power to data provides further support for the models fitted to RCS10 and RCS18 (Fig. 8). The correspondence between stimulation amplitude in the model (arbitrary units) and in the data (mA) was established as described in the *Correspondence between stimulation amplitude in the model and in the data* section in the Methods. In Fig. 8, green points indicate stimulation parameters resulting in 1:2 entrainment in both model and data (where the tongues overlap). This choice is the most natural to study the relationship between entrained peak power in the model and the data. Black points indicate stimulation parameters that are inside the data 1:2 tongue, but outside the model 1:2 tongue, and thus have an entrained PSD power in the model very close to zero. This analysis mixes power prediction with tongue shape prediction, but is more conservative which is why we are presenting both results. There is a significant correlation between data and model predictions for RCS10 ($p<1\times10^{-3}$, Fig. 8B) regardless of whether the model predictions produce 1:2 entrainment or not. RCS18 had a significant correlation for model results that resulted in 1:2 entrainment ($p<0.05$, Fig. 8C), but not for all model predictions. This is due to some stimulation parameters causing 1:2 entrainment far from the natural FTG frequency falling outside of the model 1:2 tongue, where there is a lower PSD (collection of black points in Fig. 8C where the model PSD prediction is close to zero). While there were no significant correlations between model and data entrained peak power in RCS02 (Fig. 8A-B), the lack of correlation may be explained by a stronger impact on entrainment of fluctuations in the endogeneous FTG in this patient (more details in the discussion).

Discussion

Here, we studied entrainment of cortical FTG by basal ganglia deep brain stimulation, using a computational model in conjunction with sensorimotor cortex ECoG sensed from chronically implanted bidirectional interfaces in three patients with PD. We show that through fitting a model of interacting neuronal populations to off-stimulation data, we are able to predict the region of stimulation parameters (frequency and amplitude) for which 1:2 entrainment is possible. In particular, our model predicts that 1:2 entrainment is lost when stimulation amplitude is increased above a certain value. Furthermore, the 1:2 Arnold tongue is generally left leaning, implying that 1:2 entrainment can be achieved for stimulation frequencies markedly lower than twice the frequency of the natural gamma rhythm, but not for frequencies markedly higher.

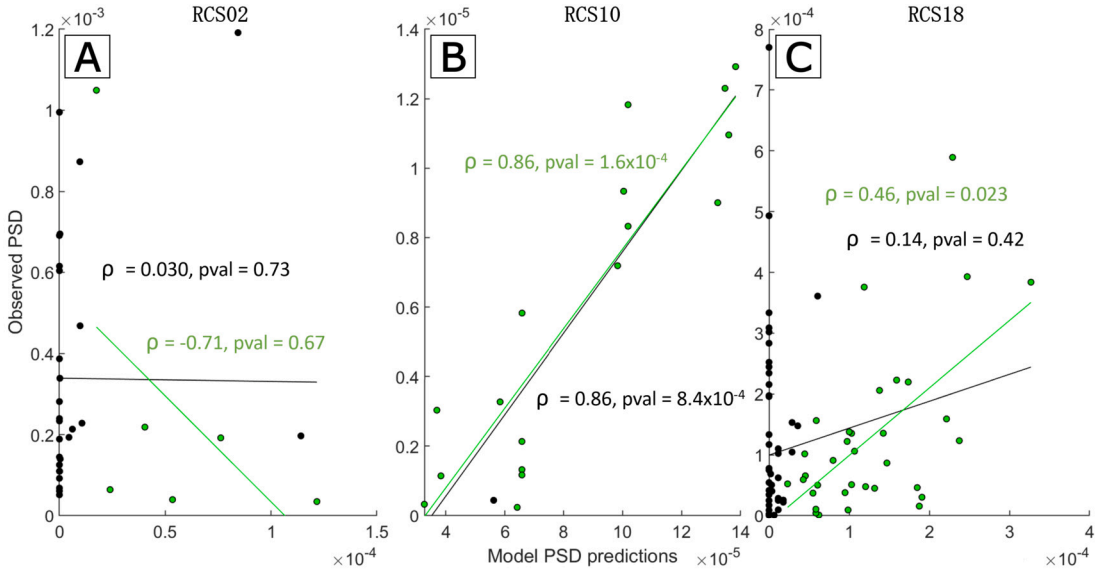

Fig. 8. Correlation between model predictions for 1:2 entrained peak power and data. Panel A is for RCS02, B for RCS10 and C for RCS18. Across the three panel, all the data points presented are stimulation parameters that resulted in 1:2 entrainment in the data. The model PSD predictions are obtained using the same stimulation parameters as in the data. Points in green represent stimulation parameters that also achieved 1:2 entrainment in the model, whereas black points did not. The green linear regression fit, ρ value and p-value (pval) are calculated using only the points resulting in 1:2 entrainment in the fitted Wilson-Cowan model. The black equivalent is calculated using all points, regardless of whether the fitted model predicted 1:2 entrainment or not. The correlations reported are Spearman's and p-values are calculated using a permutation test as outlined in the *Correspondence between stimulation amplitude in the model and in the data* section.

Lastly, the model further predicts that there would be a greater entrained gamma power at lower stimulation frequencies that result in 1:2 entrainment. Data recorded during therapeutic neurostimulation, after the modelling results were obtained, showed 1:2 Arnold tongues that generally validate these predictions. Hence, the model can capture a range of sub-harmonic entrainment features without being constrained by entrainment data. The work indicates that effects of DBS at clinically relevant stimulation parameters can be understood using the conceptual framework of a mathematical model representing interacting neural populations being externally perturbed by the periodic neurostimulation.

Entrainment and adaptive DBS

By solely analysing the presence of 1:2 entrainment, we avoid the prominent artefact at stimulation frequency. Hence, this analysis of the data provides a valuable insight into the neuronal responses to stimulation. Bounding the 1:2 tongue from above, as we lose 1:2 entrainment at increased stimulation amplitudes (all three patients at 150 Hz), provides further evidence that the gamma peak at half stimulation frequency is unlikely to be artefactual. This is aligned with the model prediction that 1:2 entrainment will be lost when amplitude is increased beyond a certain point. Additionally, the model predicts that parameter changes that result in the loss of 1:2 entrainment would see a transition to 1:1 entrainment. However, the presence of 1:1 entrainment is difficult to assess as the resulting power spectral peak can be masked by the stimulation artefact.

1:2 entrainment presents opportunities for adaptive deep brain stimulation (aDBS). aDBS relies on a closed-loop control policy where a biomarker is used to adjust DBS parameters. Cortical gamma-band activity was shown to be a promising candidate biomarker for aDBS [5, 10], and stimulation-entrained gamma has been used to control clinically successful aDBS [40]. Additionally, entrainment in the gamma frequency band has been linked with dyskinesia [5]. Moreover, 1:2 entrainment has an entirely predictable frequency, which simplifies implementation, particularly for chronic devices with limited spectral recording frequency bands (such as the Medtronic Percept).

Entrainment in the Wilson-Cowan model

1:2 entrainment is not an intrinsic property of the Wilson-Cowan model (large regions of parameter space do not lead to 1:2 entrainment). Additionally, if the parameters of the Wilson-Cowan model do produce 1:2 entrainment, the 1:2 tongue can also be right leaning or symmetrical about the central frequency. Hence, the parameters of the Wilson-Cowan model need to be tuned to reproduce the data. Among the top-ranked Wilson-Cowan fits, there is some variability between the parameter sets and the corresponding entrainment predictions (see Supplementary Materials section E.1). This demonstrates that the model parameters are non-identifiable. However, as the best fits converge on results that all include a left leaning 1:2 tongue and given the validation of some of the model predictions by follow-up recordings, we can conclude that the fitted model remains a good candidate to make predictions for future investigations. It would be possible to fit Wilson-Cowan model parameters to on-stimulation entrainment data, which may or may not reproduce off-stimulation data. This is not something we are investigating as more value is provided by predicting the response from off-stimulation fits.

While only 1:2 entrainment is investigated here, entrainment will occur at other sub-harmonics of stimulation if there is a neuronal rhythm present to entrain and the corresponding Arnold tongue is large enough to encompass the neuronal rhythm. Similarly to 1:2 entrainment, sub-harmonic entrainment at every harmonic of stimulation is not an intrinsic property of Wilson-Cowan models. However, other sub-harmonic entrainment ratios can be observed for certain model parameter sets. By increasing stimulation frequency, for example to around 225 Hz, it would be possible to investigate other sub-harmonic entrainment ratios such as 1:3 entrainment of the FTG rhythm.

The observation of the highest spectral peaks occurring at the lowest frequencies of stimulation in the model may be somewhat counter-intuitive, since one could expect more stimulation energy to provide more oscillatory power. However, due to the increased time between successive pulses of stimulation at lower frequencies, the trajectory of the population activity covers a larger distance in phase space (see Supplementary Materials section E.4, specifically Supplementary Materials Fig S.8 for more details on population activity vector fields and trajecto-

ries). This means that the range of values that activity reaches for each population is greater, producing a higher power spectral peak for the given resultant frequency. Population activity having a larger range can also be interpreted as there being greater synchrony of neurons within the populations, as increased peak firing rates and decreased minima suggest more neurons are firing together.

Because the endogenous FTG is stronger for RCS02 and stimulation amplitude is lower, more variability in the on-stimulation entrained power is expected, which may explain the worse model performance for this patient (Fig. 6 and 8). Specifically, the off-stimulation features of RCS02 (Supplementary Materials Fig S.2A) show a higher gamma peak in the PSD, a larger peak amplitude of the envelope PDF, and a shallower slope at lower amplitudes of the envelope PDF than RCS10 (Fig. 4) and RCS18 (Supplementary Materials Fig S.2B). Therefore, it is expected to be more difficult to perturb the underlying oscillators away from the natural gamma frequency of the network, which leads to a 1:2 tongue with a much smaller width over the stimulation frequency axis. Given that the stimulation amplitude used for RCS02 is also smaller than for the other patients (see Fig. 6), the strength of the endogenous FTG relative to stimulation amplitude is significantly greater, and natural fluctuations in the endogenous FTG have a larger impact on the power measured. This leads to more variability in Fig. 6C and a worse correspondence with the fitted model. However, the fitted model still manages to predict a 1:2 tongue with a smaller area and a significantly lower top boundary compared to the other models, as observed in the entrainment data. Hence, the model is able to predict features of the 1:2 tongue even with stronger endogenous rhythms.

Our modelling approach is based on ECoG recordings, but alternatives could be explored in future work. While non-invasive electroencephalography (EEG) has been used to study cortical gamma cross-frequency coupling with DBS [39], ECoG recordings have a markedly better signal-to-noise ratio. Thus, whether FTG features obtained from EEG are sufficiently accurate to enable reliable FTG entrainment predictions through model fitting requires further investigation.

Study limitations

As a pilot study, there was no systematic mapping of tongue boundaries, with large regions of untested parameters for some patients and a non-standardised approach to selecting stimulation parameters. Both of these shortcomings will be the focus of further investigations. However, extensive mapping of the 1:2 Arnold tongue boundary may be limited by patient fatigue and discomfort as some parameters tested are subtherapeutic and thus likely to lead to brief exacerbation of motor signs. In particular, there are relatively few data points to show the disappearance of 1:2 entrainment at high stimulation amplitudes (see Fig. 6C, F, and I). At these higher amplitudes, patients often experienced adverse effects which could be mildly unpleasant. Hence, following the documentation of loss or reduction of entrainment, higher amplitudes were not explored further. Provided these adverse effects can be better mitigated, the disappearance of 1:2 entrainment at high stimulation amplitudes will be confirmed in future studies.

Additionally, the absence of data on the clinical significance of gamma entrainment is a major limitation of this study and will be a focus for future work. However, Oehrn et al. recently reported that FTG power entrained at the half stimulation harmonic can predict hyperkinetic states in PD patients at home, and was identified as the optimal control signal for aDBS aimed at reducing residual motor fluctuations [40]. FTG-controlled aDBS resulted in improved motor symptoms and quality of life during normal daily activities at home compared to standard-of-care continuous stimulation.

Given that ECoG data represents the activity of populations of neurons, the Wilson-Cowan model (a neural population model) is the appropriate level of description for this type of data. However, this doesn't allow us to observe or model the behaviour of individual neurons in response to stimulation and during 1:2 entrainment. Our approach is nonetheless adequate to predict stimulation parameters leading to 1:2 entrainment. Additionally, we have not included a population to represent the basal ganglia in our model. This was because there was no consistent subcortical off-stimulation gamma peak to fit a Wilson-Cowan network to for these patients. Subcortical narrowband oscillations in the basal ganglia have been recorded in long term recordings in other patients [10]. It may also be possible to observe 1:2 entrainment in the subcortex and while this study only considers cortical populations, the methodology presented here can be translated to any network of interacting excitatory and inhibitory populations of neurons. Furthermore, we did not consider plasticity in our model. While short-term response to stimulation (such as during the follow-up on-stimulation recordings reported here) can be described by models without plasticity, the several months of chronic stimulation between the prestimulation and follow-up recordings are likely to have led to plasticity, which we did not account for here.

The orthodromic projections from STN or pallidum to cortex are all polysynaptic, and whether the effect of basal ganglia DBS on cortex is excitatory or inhibitory is not well understood. There exist strong connections from STN to GPe [41,42] and direct GABAergic projections from ChAT (choline acetyltransferase) and prototypic neurons from the GPe to the cortex [42]. Hence, stimulation from these two sites may act primarily on inhibitory populations of the cortex. However, there is not sufficient understanding of the effects of DBS on the basal ganglia as well as the exact nature of the projections from the basal ganglia to the cortex. It is also unclear how antidromic activation of the stimulation targets would effect the motor cortex. To accommodate for this uncertainty, we consider DBS with both GABAergic and glutamergic tendencies (see Supplementary Materials section E.5). Stimulation to our fitted models consistently produces 1:2 entrainment with a left leaning tongue regardless of the population being stimulated. Hence, this choice is inconsequential and the presence of 1:2 entrainment is more specific to the dynamics of the cortical populations than the excitatory bias of the stimulating pulse.

Implications

This work demonstrates that brain rhythms can have nonlinear responses to stimulation, such as entrainment at harmonics of stimulation frequency, and non-monotonic rhythmic responses to stimulation amplitude. We argue against the simple view that only brain rhythms close to the stimulation frequency can be entrained (through 1:1 entrainment).

These findings might have implications across frequencies. 1:1 entrainment has been reported for example in the alpha band through single pulse transcranial magnetic stimulation when treating depression [16], with rhythmic visual stimulation [17], and with tACS [43]. If rhythms can lock to harmonics of stimulation frequency, as supported by this study, it is possible that current stimulation protocols targeting any frequency band could induce unexpected responses at sub- or supra-harmonics of the stimulation frequency. Thus, when designing stimulation protocols one should be aware of potential ramifications of stimulation on neuronal rhythms at multiple frequencies. For instance, stimulation targeting lower frequency oscillations, such as beta rhythms, may be able to entrain gamma at a 2:1 rotation number, or even alpha at a 1:2 rotation number. Similar considerations have been employed when designing stimulation protocols in a canine with epilepsy [44]. More recently, a principled approach to selectively promote rhythms close to the stimulation frequency while preventing entrainment at sub- and super-harmonics was put forward in [45].

Conclusion

We show that for certain network parameters, simple neural circuits can support 1:2 entrainment to DBS. Our fitted Wilson-Cowan model

provides theoretical evidence for a neural circuit origin of 1:2 entrainment of cortical FTG oscillation to high-frequency DBS in PD patients. Furthermore, it predicts a larger region of stimulation parameters, at frequencies corresponding to less than twice the natural frequency of the system, for which 1:2 entrainment would be observed. These results are validated by 1:2 Arnold tongue charting from the same patients to whom the model was fitted.

Understanding the variety of effects of stimulation on brain rhythms would provide valuable insights into designing stimulation protocols to provide maximum therapeutic benefit with minimal side effects. This model provides a first step to predicting these responses. Computational models enable us to experiment with a variety of waveforms without the burdensome tests and validation that would be associated with in patient trials. Prediction of the neuronal responses to stimulation is a fundamental step in the design of future therapeutic protocols. Our model predicts that these responses are not a simple one-for-one mapping of stimulation frequency and amplitudes to brain network activity and that stimulation may have significant effects, even when the stimulation frequency is outside of the frequency band of interest.

Funding information

JS and TD are supported by DARPA HR0011- 20-2-0028 Manipulating and Optimising Brain Rhythms for Enhancement of Sleep (Morpheus) and the UK Medical Research Council grant MC_UU_00003/3. MO and PS are supported by NIH/NINDS award R01NS090913. JA is supported by Swiss National Science Foundation (Early Postdoc Mobility – P2BEP3_188140). SL is supported by NIH award K23NS120037. RB and BD are supported by Medical Research Council grant MC_UU_00003/1. SC is supported by NIH/NINDS award number F32NS129627. Content represents views of the authors and not the funders.

CRediT authorship contribution statement

James J. Sermon: Conceptualization, Investigation, Methodology, Validation, Visualization, Writing – original draft, Writing – review & editing. **Maria Olaru:** Conceptualization, Data curation, Investigation, Writing – original draft, Writing – review & editing. **Juan Ansó:** Conceptualization, Data curation, Methodology, Writing – review & editing. **Stephanie Cernera:** Data curation, Investigation, Writing – original draft, Writing – review & editing. **Simon Little:** Writing – review & editing. **Maria Shcherbakova:** Data curation, Investigation, Writing – original draft, Writing – review & editing. **Rafal Bogacz:** Conceptualization, Funding acquisition, Supervision, Writing – review & editing. **Philip A. Starr:** Conceptualization, Funding acquisition, Resources, Supervision, Writing – review & editing. **Timothy Denison:** Conceptualization, Funding acquisition, Supervision, Writing – review & editing. **Benoit Duchet:** Conceptualization, Investigation, Methodology, Supervision, Writing – review & editing.

Declaration of competing interest

PS receives research support from Medtronic Inc. (providing investigational devices free of charge). SL is a scientific advisor for RuneLabs. The University of Oxford has research agreements with Bioinduction Ltd. TD has stock ownership (< 1%) and business relationships with Bioinduction for research tool design and deployment, as well as being an advisor for Synchron and Cortec Neuro.

Data availability

The data will be made available upon reasonable request to Philip.Starr@ucsf.edu.

Acknowledgements

The authors are thankful to Huiling Tan for providing helpful comments on the manuscript. The authors would like to acknowledge the use of the University of Oxford Advanced Research Computing (ARC) facility in carrying out this work. http://dx.doi.org/10.5281/zenodo.22558.

Appendix. Supplementary material

Supplementary material related to this article can be found online at https://doi.org/10.1016/j.brs.2023.08.026.

References

[1] Koller William, Pahwa Rajesh, Busenbark Karen, Hubble Jean, Wilkinson Steve, Lang Anthony, et al. High-frequency unilateral thalamic stimulation in the treatment of essential and parkinsonian tremor. Ann Neurol 1997;42.
[2] Koeglsperger Thomas, Palleis Carla, Hell Franz, Mehrkens Jan H, Bötzel Kai. Deep brain stimulation programming for movement disorders: current concepts and evidence-based strategies. Front Neurol 2019;10.
[3] Bosman Conrado A, Lansink Carien S, Pennartz Cyriel MA. Functions of gamma-band synchronization in cognition: from single circuits to functional diversity across cortical and subcortical systems. Eur J Neurosci Jun. 2014;39(11):1982–99.
[4] Nowak Magdalena, Zich Catharina, Stagg Charlotte J. Motor cortical gamma oscillations: what have we learnt and where are we headed? Curr Behav Neurosci Rep Apr. 2018;5(2):136–42.
[5] Swann Nicole C, De Hemptinne Coralie, Miocinovic Svjetlana, Qasim Salman, Wang Sarah S, Ziman Nathan, Ostrem Jill L, et al. Gamma oscillations in the hyperkinetic state detected with chronic human brain recordings in Parkinson's disease. J Neurosci Jun. 2016;36(24):6445–58.
[6] Wiest C, Torrecillos F, Tinkhauser G, Pogosyan A, Morgante F, Pereira EA, et al. Finely-tuned gamma oscillations: spectral characteristics and links to dyskinesia. Elsevier Enhanced Reader. Exp Neurol 2022;351:113999.
[7] Cassidy Michael, Mazzone Paolo, Oliviero Antonio, Insola Angelo, Tonali Pietro, Di Lazzaro Vincenzo, et al. Movement-related changes in synchronization in the human basal ganglia. Brain Jun. 2002;125(6):1235–46.
[8] Williams David, Tijssen Marina, Van Bruggen Gerard, Bosch Andries, Insola Angelo, Di Lazzaro Vincenzo, Mazzone Paolo, et al. Dopamine-dependent changes in the functional connectivity between basal ganglia and cerebral cortex in humans. Brain Jul. 2002;125(7):1558–69.
[9] de Hemptinne Coralie, Wang Doris D, Miocinovic Svjetlana, Chen Witney, Ostrem Jill L, Starr Philip A. Pallidal thermolesion unleashes gamma oscillations in the motor cortex in Parkinson's disease. Mov Disord Jun. 2019;34(6):903–11.
[10] Gilron Ro'ee, Little Simon, Perrone Randy, Wilt Robert, de Hemptinne Coralie, Yaroshinsky Maria S, et al. Long-term wireless streaming of neural recordings for circuit discovery and adaptive stimulation in individuals with Parkinson's disease. Nat Biotechnol May 2021;39(9):1078–85.
[11] Halje Pär, Tamtè Martin, Richter Ulrike, Mohammed Mohsin, Angela Cenci M, Petersson Per. Levodopa-induced dyskinesia is strongly associated with resonant cortical oscillations. J Neurosci Nov. 2012;32(47):16541–51.
[12] Güttler Christopher, Altschüler Jennifer, Tanev Kaloyan, Böckmann Saskia, Kersten Haumesser Jens, Nikulin Vadim V, et al. Levodopa-induced dyskinesia are mediated by cortical gamma oscillations in experimental parkinsonism. Mov Disord Apr. 2021;36(4):927–37.
[13] Guerra Andrea, Colella Donato, Giangrosso Margherita, Cannavacciuolo Antonio, Paparella Giulia, Fabbrini Giovanni, et al. Driving motor cortex oscillations modulates bradykinesia in Parkinson's disease. Brain Jul. 2021.
[14] Swann Nicole C, De Hemptinne Coralie, Thompson Margaret C, Miocinovic Svjetlana, Miller Andrew M, Gilron Ro'Ee, et al. Adaptive deep brain stimulation for Parkinson's disease using motor cortex sensing. J Neural Eng May 2018;15(4).
[15] Arnol'd VI. Remarks on the perturbation theory for problems of Mathieu type. Russ Math Surv Aug. 1983;38(4):215–33.
[16] Fröhlich Flavio. Tuning out the blues – Thalamo-cortical rhythms as a successful target for treating depression. Brain Stimul: Basic, Transl, Clin Res Neuromodulation nov 2015;8(6):1007–9.
[17] Notbohm Annika, Kurths Jürgen, Herrmann Christoph S. Modification of brain oscillations via rhythmic light stimulation provides evidence for entrainment but not for superposition of event-related responses. Front Human Neurosci Feb. 2016;10(FEB2016).
[18] Ali Mohsin M, Sellers Kristin K, Fröhlich Flavio. Transcranial alternating current stimulation modulates large-scale cortical network activity by network resonance. J Neurosci Jul. 2013;33(27):11262–75.
[19] Hanslmayr Simon, Axmacher Nikolai, Inman Cory S. Modulating human memory via entrainment of brain oscillations. Trends Neurosci 2019;42(7):485–99. https://doi.org/10.1016/j.tins.2019.04.004.
[20] Wilson Hugh R, Cowan Jack D. Excitatory and inhibitory interactions in localized populations of model neurons. Biophys J 1972;12(1):1–24.

[21] Cowan Jack D, Neuman Jeremy, van Drongelen Wim. Wilson–Cowan equations for neocortical dynamics. J Math Neurosci Jan. 2016;6(1).
[22] Lea-Carnall Caroline A, Montemurro Marcelo A, Trujillo-Barreto Nelson J, Parkes Laura M, El-Deredy Wael. Cortical resonance frequencies emerge from network size and connectivity. PLoS Comput Biol Feb. 2016;12(2):e1004740.
[23] Velarde Osvaldo Matías, Mato Germán, Dellavale Damián. Mechanisms for pattern specificity of deep-brain stimulation in Parkinson's disease. PLoS ONE Aug. 2017;12(8):e0182884.
[24] Cutsuridis Vassilis. Multiscale models of brain disorders. Springer; 2019.
[25] Yousif Nada, Mace Michael, Pavese Nicola, Borisyuk Roman, Nandi Dipankar, Bain Peter. A network model of local field potential activity in essential tremor and the impact of deep brain stimulation. PLoS Comput Biol Jan. 2017;13(1):e1005326.
[26] Duchet Benoit, Weerasinghe Gihan, Cagnan Hayriye, Brown Peter, Bick Christian, Bogacz Rafal. Phase-dependence of response curves to deep brain stimulation and their relationship: from essential tremor patient data to a Wilson–Cowan model. J Math Neurosci Dec. 2020;10(1).
[27] Pérez-Cervera Alberto, M-Seara Tere, Huguet Gemma. A geometric approach to phase response curves and its numerical computation through the parameterization method. J Nonlinear Sci Sep. 2019;29(6):2877–910.
[28] Papasavvas Christoforos A, Trevelyan Andrew J, Kaiser Marcus, Wang Yujiang. Divisive gain modulation enables flexible and rapid entrainment in a neocortical microcircuit model. J Neurophysiol Mar. 2020;123(3):1133–43.
[29] Veltz Romain, Sejnowski Terrence J. Periodic forcing of inhibition-stabilized networks: nonlinear resonances and phase-amplitude coupling. Neural Comput Dec. 2015;27(12):2477–509.
[30] Hoppensteadt Frank C, Izhikevich Eugene M. Thalamo-cortical interactions modeled by weakly connected oscillators: could the brain use FM radio principles? Biosystems Nov. 1998;48:85–94.
[31] Borisyuk Roman M, Kirillov Alexandr B. Bifurcation analysis of a neural network model. Biol Cybern Feb. 1992;66(4):319–25.
[32] Onslow Angela CE, Jones Matthew W, Bogacz Rafal. A canonical circuit for generating phase-amplitude coupling. PLoS ONE Aug. 2014;9(8):e102591.
[33] Okun Michael S, Fernandez Hubert H, Wu Samuel S, Kirsch-Darrow Lindsey, Bowers Dawn, Bova Frank, et al. Cognition and mood in Parkinson's disease in subthalamic nucleus versus globus pallidus interna deep brain stimulation: the compare trial. Ann Neurol 2009;65.
[34] Follett Kenneth A, Weaver Frances M, Stern Matthew, Hur Kwan, Harris Crystal L, Luo Ping, et al. Pallidal versus subthalamic deep-brain stimulation for Parkinson's disease. N Engl J Med 2010;362.
[35] Starr Philip A. Placement of deep brain stimulators into the subthalamic nucleus or globus pallidus internus: technical approach. Stereotact Funct Neurosurg 2002;79.
[36] Shahlaie Kiarash, Larson Paul S, Starr Philip A. Intraoperative computed tomography for deep brain stimulation surgery: technique and accuracy assessment. Neurosurgery 2011;68.
[37] Swann Nicole C, De Hemptinne Coralie, Miocinovic Svjetlana, Qasim Salman, Ostrem Jill L, Galifianakis Nicholas B, et al. Chronic multisite brain recordings from a totally implantable bidirectional neural interface: experience in 5 patients with Parkinson's disease. J Neurosurg 2018;128.
[38] Duchet Benoit, Ghezzi Filippo, Weerasinghe Gihan, Tinkhauser Gerd, Kühn AA, Brown Peter, et al. Average beta burst duration profiles provide a signature of dynamical changes between the on and off medication states in Parkinson's disease. PLoS Comput Biol Jul. 2021;17(7):e1009116.
[39] Muthuraman Muthuraman, Bange Manuel, Koirala Nabin, Ciolac Dumitru, Pintea Bogdan, Glaser Martin, et al. Cross-frequency coupling between gamma oscillations and deep brain stimulation frequency in Parkinson's disease. Brain Dec. 2020;143(11):3393–407.
[40] Oehrn Carina R, Cernera Stephanie, Hammer Lauren H, Shcherbakova Maria, Yao Jiaang, et al. Personalized chronic adaptive deep brain stimulation outperforms conventional stimulation in Parkinson's disease. 2023. MedRxiv.
[41] Calabresi P, Picconi B, Tozzi A, Ghiglieri V, Di Filippo M. Direct and indirect pathways of basal ganglia: a critical reappraisal. Nat Neurosci 2014;17(8):1022–30. https://doi.org/10.1038/nn.3743.
[42] Dong Jie, Hawes Sarah, Wu Junbing, Le Weidong, Cai Huaibin. Connectivity and functionality of the globus pallidus externa under normal conditions and Parkinson's disease. Front Neural Circuits 2021;15(8):3.
[43] Huang Wei A, Stitt Iain M, Negahbani Ehsan, Passey DJ, Ahn Sangtae, et al. Transcranial alternating current stimulation entrains alpha oscillations by preferential phase synchronization of fast-spiking cortical neurons to stimulation waveform. Nat Commun May 2021;12(1):1–20.
[44] Zamora Mayela, Meller Sebastian, Kajin Filip, Sermon James J, Toth Robert, Benjaber Moaad, et al. Report: embedding "digital chronotherapy" into medical devices—a canine validation for controlling status epilepticus through multi-scale rhythmic brain stimulation. Front Neurosci Sep. 2021;15:1196.
[45] Duchet Benoit, Sermon James J, Weerasinghe Gihan, Denison Timothy, Bogacz Rafal. How to entrain a selected neuronal rhythm but not others: open-loop dithered brain stimulation for selective entrainment. J Neural Eng Apr. 2023;20(2):026003.